

Highly Stretchable Conductor Inspired by Compliant Mechanism

Zhilai Lu, Yinjun Deng, Xintong Zhou, Lei He, Jianan Song,* Qingshan Wang, Jianfang Xia,* Linpeng Liu, Farid A. Hammad, and Yanling Tian

Flexible and stretchable conductors have invaluable applications in multiple domains, such as sensors, displays, and electronic skins. The stable conductance exhibited by conductors when subjected to diverse forms of deformation, such as tensile stress, curvature, or torsion, represents a fundamental characteristic. Attaining high conductivity and stretchability simultaneously in conductive materials is a formidable challenge, owing to inherent constraints in materials found in nature. To overcome this problem, an innovative approach of structurally designing conductors using existing materials to achieve high deformability and stretchability, i.e. stretchable conductors inspired by a compliant mechanism is proposed in this paper. Thus, a novel stretchable conductor inspired by flexible mechanisms is introduced. Unlike stretchable conductors based on Kirigami structures, the stretchable conductor based on flexible mechanisms can achieve large in-plane deformation within the material's strength limit. The concept and design process of the highly deformable stretchable conductor inspired by flexible mechanisms are presented in this paper. Experimental results show that the resistance change ratio of the conductor remains within 0.05% during the 0–200% strain process. The consistency and durability of the conductor during stretching deformation are also confirmed through 500 repetitions of the test. Additionally, the experiments with the electric motor and light-emitting diode (LED) light confirm the conductor's ability to maintain a stable current.

essential components in flexible electronics.^[1] They can be used as the tensile connectors of sensors,^[2–5] displays, circuits,^[6,7] and e-skins,^[5] among other things.^[8–13] Good electrical conductivity and stability when subjected to large deformations are essential qualities of stretchable conductors. Conventional conductive materials, like metals, have extraordinary conductivity but limited maximum tensile strain (around 2%). On the contrary, rubbers with large deformation performance have poor electrical conductivity. The intrinsic contradiction between conductivity and tensile capacity hinders the development of flexible conductors. In order to solve this contradiction, there are two possible solutions, namely, to improve the conductivity of flexible materials and to enhance the stretchability of conductive materials.^[14,15] These two ideas correspond to two ongoing research directions: developing conductive rubbers with doped conductive fillers, such as copper nanowires^[16] and graphene,^[17] and increasing metals' stretchability with specific

structures, such as wavy structures^[18,19] and Kirigami structures.^[2,20–23]

In addition, some researchers have integrated the advantages of both approaches by utilizing the structural

1. Introduction


Conductors that can maintain stable conductivity while undergoing deformation, such as stretching, bending, or twisting, are

Z. Lu, Y. Deng, X. Zhou, L. He, J. Song, Q. Wang, J. Xia
State Key Laboratory of Precision Manufacturing for Extreme Service Performance, College of Mechanical and Electrical Engineering
Central South University
Changsha 410083, China
E-mail: songjianan@csu.edu.cn; xia-jianfang@csu.edu.cn

L. Liu
Central South University
No. 932, Lushan road, Changsha 12570, China

F. A. Hammad
Mechanical Power Engineering Department
Faculty of Engineering
Tanta University
Tanta 31521, Egypt

Y. Tian
School of Engineering
University of Warwick
Coventry CV4 7AL, UK

 The ORCID identification number(s) for the author(s) of this article can be found under <https://doi.org/10.1002/aelm.202300343>

© 2023 The Authors. Advanced Electronic Materials published by Wiley-VCH GmbH. This is an open access article under the terms of the Creative Commons Attribution License, which permits use, distribution and reproduction in any medium, provided the original work is properly cited.

DOI: 10.1002/aelm.202300343

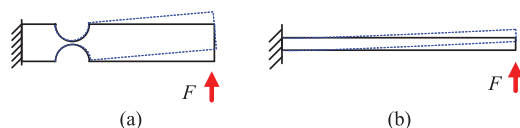


Figure 1. Two kinds of flexure hinges in compliant mechanism: a) Notch-type flexure hinge, and b) leaf-type flexure hinge.

arrangement of mixed materials.^[24] For example, Wang et al. proposed a Kirigami-patterned stretchable conductive film with carbon nanotube (CNT) networks.^[21] The maximum elongation of the film can reach 380% with stable conductivity. Shyu et al. found that Kirigami-inspired notches can prevent unpredictable local failure and increase the ultimate strain of the rigid nanocomposite sheet from 4% to 370%.^[25] Kirigami structures are also used in large deformation strain sensors,^[17,26] solar tracking systems,^[27] supercapacitors,^[28] and other devices,^[29] due to their high performance in increasing the structural compliance of these devices.

However, it should be noted that the out-of-plane deformation of Kirigami-based structures is inevitable during the elongation process. This intrinsic characteristic can be employed to adjust the working parameters in cases where patches are used as functional modules. However, the out-of-plane deformation can impede the tensile strain capacity of Kirigami structures when they are used as connectors fitting the surface of human skin or semiconductor substrates.

In this paper, we propose a novel kind of stretchable conductors inspired by compliant mechanism (CM).^[30] Compliant mechanism, also known as flexible mechanism, employs material deformation to transmit or convert motion, force, or energy. **Figure 1** illustrates two commonly used types of flexure hinges in compliant mechanisms: the notch-type and leaf-type flexure hinges. These hinges are intended to replace rigid hinges like bearings, thus eliminating clearance and friction that are inevitable in traditional mechanisms. Compliant mechanisms find widespread application in precision engineering, robotics, intelligent structures, and other fields.^[31–34] In the design process of compliant mechanisms, the flexure hinge is critical for achieving the desired mechanism design.^[35–37] The configuration and size parameters of flexure hinges directly affect the motion characteristics of the mechanism. The notch-type flexure hinge can achieve higher motion accuracy, while the leaf-type flexure hinge can achieve a larger motion range, making them suitable for different application scenarios.

Compared with conductors based on Kirigami structures, stretchable conductors based on compliant mechanisms (CMs) can achieve a large elongation capability without out-of-plane deformation, thanks to their monolithic structure and in-plane configuration. It offers in-plane deformation, thereby enhancing its compactness when connected to substrates during operation. For example, when utilized in wearable electronic devices like data gloves^[38] by printing the structure onto the surface of a stretchable substrate, or in flexible circuits^[39], the conductor adheres to the substrates without detachment, resulting in improved detection precision. Therefore, a novel kind of stretchable conductor can be obtained by designing a conductor with the design concept of compliant mechanisms. Furthermore, with the advances

in laser processing technology, an ultraviolet laser is used to pattern the designed structure.

The remainder of this paper is organized as follows. We provide a detailed description of our proposed stretchable conductor based on compliant mechanism. We begin by introducing the design concept and key parameters of compliant mechanisms, followed by the fabrication process of the proposed stretchable conductor. We then present the experimental results and performance evaluation of the fabricated conductor. Finally, we discuss the potential applications and future developments of CM-based stretchable conductors.

1.1. Design of Compliant Mechanism-Based Conductors

For flexible conductors, the primary issue that must be addressed is the contradiction between stretchability and conductivity. To reduce the variation in a conductor's conductivity during large deformation, this paper adopts the concept of a compliant mechanism. Such a mechanism leverages a material's deformation to transfer force or motion, much like the classic example of the bow and arrow. By substituting flexure hinges for rigid hinges, such as revolute joints, clearance and friction can be avoided. As a result, compliant mechanisms offer improved motion precision, making them especially well-suited for designing flat maple structures.

To meet the design requirements for a plane flexible mechanism, the pseudo-rigid-body model (PRBM) is a commonly used method for rigid structural transformation.^[30] While the topological optimization method can provide better force transmission paths, it lacks design efficiency and processing convenience. According to the PRBM approach, each flexure hinge can be kinematically equivalent to an ideal single-axis revolute joint with a torsional spring. By using the equivalent substitution method, a rigid mechanism can be efficiently transformed into a compliant mechanism. Moreover, arranging simple mechanisms in a series and/or parallel configuration can improve the overall device's performance. Specifically, a serial chain can enhance the flexibility and deformation ability of the mechanism, while a parallel structure can ensure its stiffness and stability. According to Pham and Chen,^[40] the stiffness of a parallel connection system can be obtained by $K = \sum_i K_i$, where K_i is the individual stiffness of a flexible joint. The compliance (the reciprocal of stiffness) of a serial connection system can be calculated as $C = \frac{1}{K} = \sum_i \frac{1}{K_i}$. Furthermore, some basic concepts can be listed as follows: a flexible unit can be a joint or a linkage, a serial chain is a serial connection of flexible units, and a parallel mechanism is a parallel connection of serial chains.

To apply the advantages of flexible mechanisms to the design of stretchable conductors, it is necessary to consider the requirements of flexible conductors and the characteristics of flexible mechanisms.

To clearly illustrate the specific design steps of stretchable conductors based on compliant mechanisms, three examples will be used for demonstration:

Step 1: Select suitable flexible units.

The first step in designing a stretchable conductor based on compliant mechanism is to select appropriate flexible units according to the usage requirements, including flexible hinges and

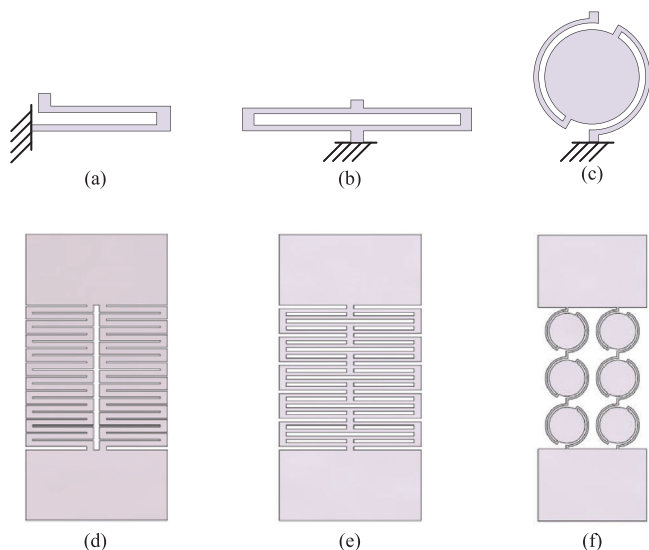


Figure 2. Three deformable structures (a)–(c) that fulfill distinct requirements and their corresponding stretchable systems (d)–(f).

linkages. For most stretchable conductors, the key is to ensure their stretchability, so leaf-spring-type flexible hinges as illustrated in Figure 1b are more suitable because they can provide greater deformation capacity before failure.

Step 2: Construct deformable structure.

Construct a deformable structure that can meet the usage requirements with the leaf-spring-type flexible hinge as the main flexible unit. The key to the design is to make good use of the bending deformation capacity of the leaf-spring-type flexible hinge and ensure the compactness of the structure. Three deformable structures are illustrated in Figure 2a–c. Figure 2a utilizes the folding of the leaf-spring-type flexible hinge to achieve greater longitudinal deformation capacity in a smaller lateral space. Figure 2b eliminates the coupling error in the non-functional direction of the structure by arranging the folding structure symmetrically as in Figure 2a. Figure 2c uses a bent leaf-spring-type flexible hinge, and the central island structure rotates during stretching, which is suitable for semiconductor devices composed of brittle materials.

Step 3: Design serial and/or parallel system.

The next step in designing a stretchable conductor based on a flexible mechanism is to connect the previously designed deformable structures in series or parallel according to usage requirements to form a stretchable system with reasonable stretch performance, stability, or special structure. The three stretchable systems in Figure 2d–f correspond to the three deformable structures in Figure 2, respectively. The stretchable conductor shown in Figure 2f is composed of a combination of six island-like structures as illustrated in Figure 2c. This system not only enables large deformations of the stretchable conductor, but also allows for the rotation of sensor components made of brittle materials such as silicon on the islands.

Step 4: Performance verification and optimization.

Upon completion of the structural design, the main design work of the stretchable conductor based on flexible mechanisms was completed. In order to verify the performance of the de-

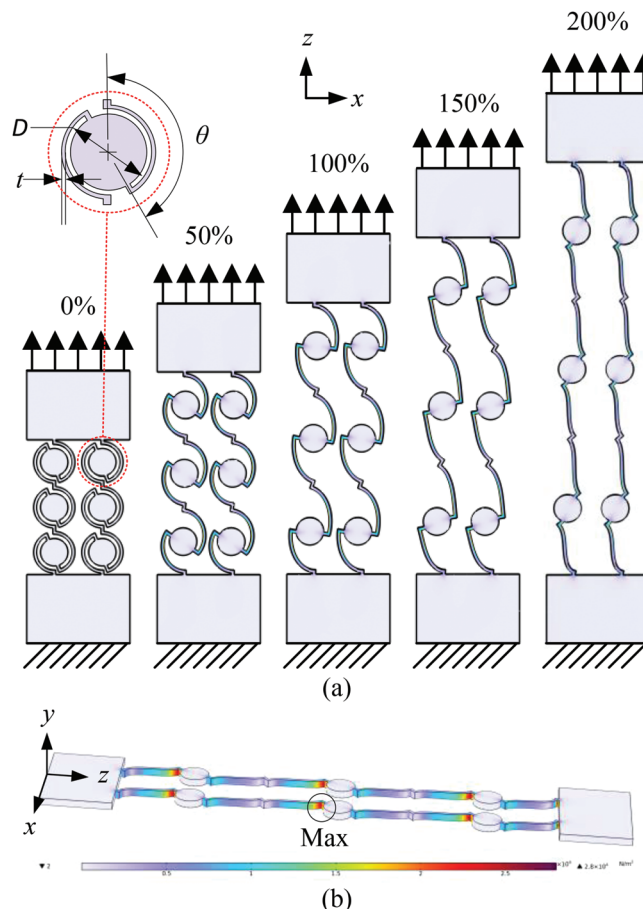


Figure 3. The FEA results: a) Deformation of the stretchable conductor under different tensile deformations; b) the stress contour map of the stretchable conductor during the deformation process.

signed stretchable conductor and optimize its size parameters according to usage requirements, finite element analysis (FEA) of the stretchability was conducted using COMSOL software. The Solidworks-based parameterized 3D model was imported into COMSOL, and the solid mechanics module was selected under structural mechanics in COMSOL. A linear elastic material was chosen, and the lower part of the structure was fixed with fixed constraints, as shown in Figure 3. Then, the stretchable conductor was stretched by giving a specified stretch distance to the other side of the structure. It should be noted that for large deformation simulations, the geometric nonlinearity option in the steady-state must be selected.

The material parameters used in the simulation are shown in Table 1. It should be noted that these parameters are only for reference due to the impact of material ratio on the properties of the conductive material. In the subsequent process of size

Table 1. Material property adopted in the finite element analysis.

Density [kg/m ³]	Young modulus [kPa]	Poisson's ratio
960	100	0.3

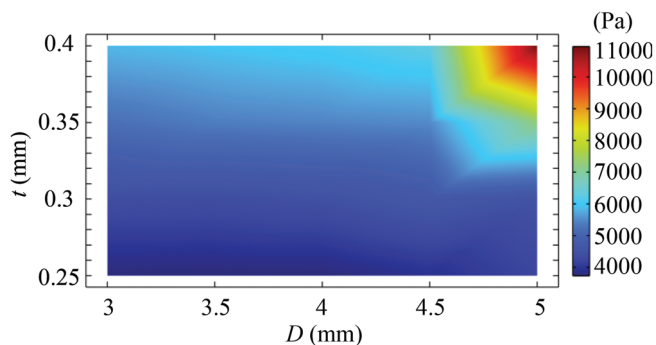


Figure 4. The FEA results: maximum stress with different parameters

optimization, the relative change of the maximum stress value will be used as the boundary condition for the size optimization.

The simulation results are presented in Figure 3, where Figure 3a illustrates the deformation of the stretchable conductor under different tensile deformations. During the stretching process, the circular spring-shaped flexible hinge gradually unfolds, accompanied by the rotation of the island-like structure. The series structure increases the maximum deformation of the stretchable conductor, while the parallel structure improves the stability of the conductor during deformation. Figure 3b shows the stress contour map of the stretchable conductor during the deformation process. The simulation results indicate that the maximum stress point appears at the root of the flexible hinge.

When the maximum stress exceeds the material's allowable stress, the failure of the stretchable conductor becomes inevitable. Additionally, for conductors that require repeated stretching and shrinking, their lifespan during the repeated deformation process is also directly influenced by the maximum stress. Therefore, using the parameter sweep function of COMSOL software, this study optimized the dimensions of the designed stretchable conductor. The optimization objective was to minimize the conductor's maximum stress under the same tensile deformation. The island-like structure has three main parameters, as shown in the zoomed-in figure in Figure 3, namely the hinge width t , the diameter D of the island, and the angle θ corresponding to the hinge length, as well as the hinge width t . Considering the limited range of the angle θ variation and the structural complexity and manufacturing difficulty, θ was set to 70° . Then, taking the hinge width t and the island diameter D as the optimization parameters, the maximum stress value of the conductor was calculated under a tensile strain of 100%. The simulation results are shown in the Figure 4. With constant material parameters and tensile strain, the maximum stress of the structure increases with an increase in radius and beam width, but the change is not significant within the range of a radius less than 4.4 mm. Considering the actual manufacturing difficulty, a radius of $D = 4$ mm and a beam width of $t = 0.4$ mm were ultimately chosen as the structural parameters.

2. Results and Discussion

Based on the dimensional parameters determined in the previous section, we fabricated a stretchable conductor utilizing an island structure and conducted performance evaluations. Please

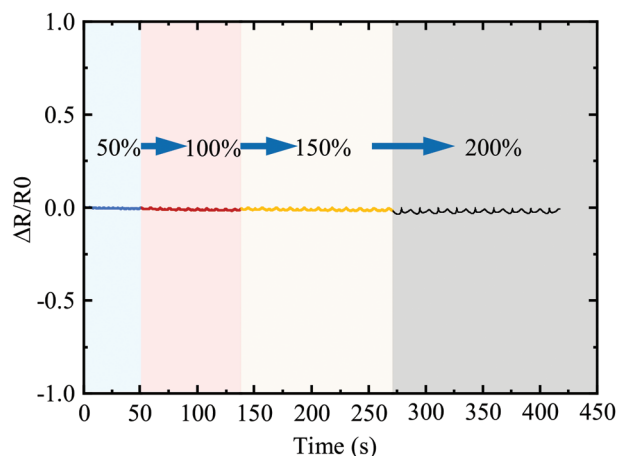


Figure 5. The resistance change ratio of the stretchable conductor under different tensile strains.

refer to the experimental section for detailed processing procedures and instrumentation. The relative resistance change ratio ($\Delta R/R_0$) is selected as an indicator of the stability of the conductivity during the tensile process, which R_0 and ΔR represent the initial resistance and the resistance change of the conductor, respectively (Figure 5).

2.1. Resistance Stability Test of Stretchable Conductor Under Tensile Deformation

In order to verify the electrical resistance stability of the designed stretchable conductor based on flexible mechanisms during deformation, we conducted a series of experiments. First, we evaluated the resistance change of the stretchable conductor under elongation deformation. During the experimental process, the conductor was elongated to 50%, 100%, 150%, and 200% of its effective length, respectively, and cycled ten times for each elongation state. The corresponding resistance change ratio $\Delta R/R_0$ of the conductor was recorded for each cycle. The experimental results are presented in the Figure 5. As shown in the results, within one stretching cycle, the resistance change ratio becomes negative with increasing strain, and the absolute value gradually increases. Specifically, the electrical resistance of the conductor decreases with increasing strain, which may be attributed to the enhanced contact between the carbon nanotubes, which serve as the conductive filler, within the composite material comprising the conductor during the stretching process. Furthermore, with the increase of maximum strain (50–200%), the change in resistance change ratio also gradually increases. However, it should be noted that even under the stretching deformation of 0–200%, the resistance change ratio of the conductor still remains within 0.05%.

Subsequently, to investigate the resistance change of the conductor under different deformation rates, we conducted experiments on the resistance change ratio of the conductor under the same maximum stretching strain (100%) but different loading rates (0.05, 0.10, 0.12, 0.15, 0.18, and 0.24 Hz). The experimental results are presented in the Figure 6. It can be observed that the variation in loading rate did not cause a significant change

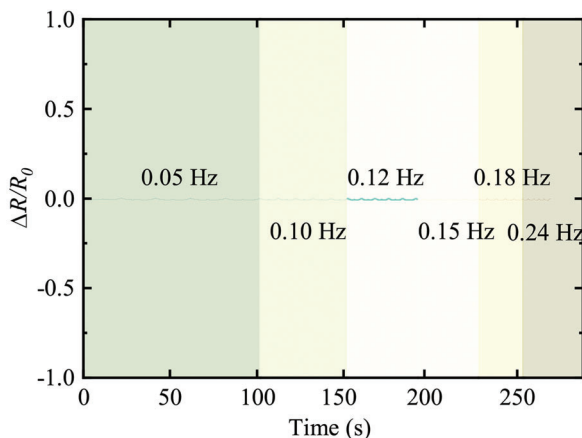


Figure 6. The resistance change ratio of the stretchable conductor under different loading rates.

in the resistance change ratio curve, verifying the ability of the conductor to maintain stable performance under different deformation rates.

In addition, to investigate the repeatability and durability of the stretchable conductor based on flexible mechanism, the resistance change under continuous stretching and releasing for 500 cycles at 100% maximum strain was tested. The experimental results are presented in the **Figure 7**. The number of cycles is denoted as N . It can be seen that the conductor exhibits highly stable repeatability and consistency during the 500-cycle test. The absolute value of resistance change ratio remains below 0.01%. This

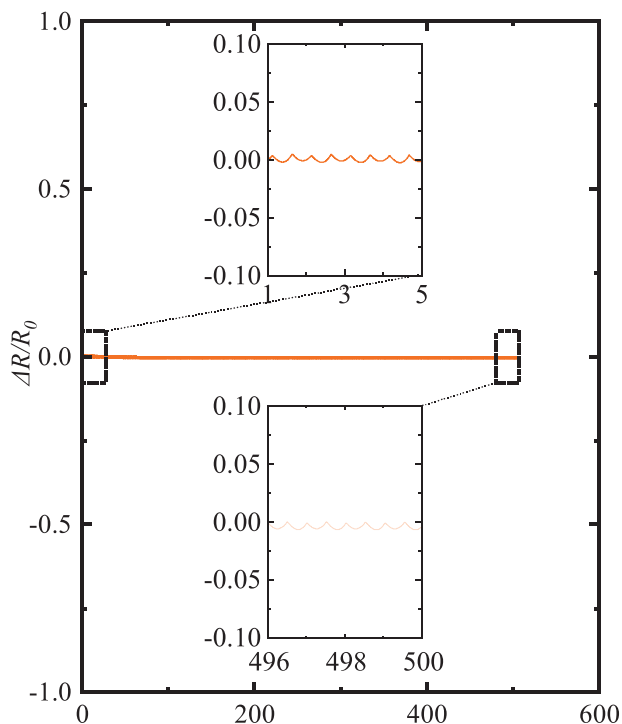


Figure 7. Repeatability and durability test results of the stretchable conductor.

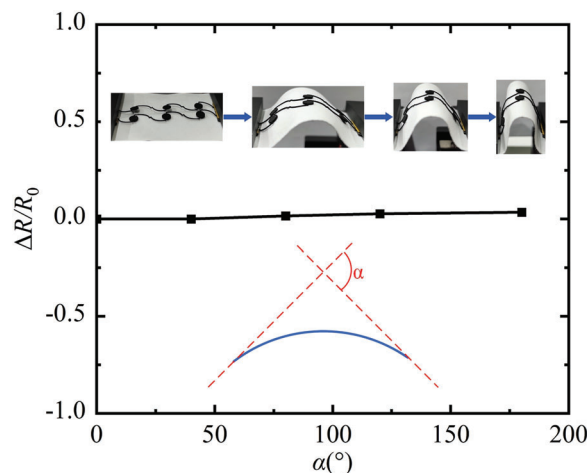


Figure 8. The resistance change ratio of the stretchable conductor under different bending angles.

also demonstrates the excellent stability and durability of the conductor under large deformations, which is a crucial characteristic for stretchable conductors.

Based on the analysis of the experimental data, the following conclusions can be drawn: The stretchable conductor based on the island-bridge structure exhibits stable resistance changes under large deformation, and the resistance does not change significantly with the degree of strain, stretching frequency, or number of strain cycles, confirming its adaptability under different stretching conditions.

2.2. Resistance Stability Test of Stretchable Conductor under Bending Deformation

In certain working conditions, it is inevitable for stretchable conductors to undergo some degree of bending deformation, in addition to tensile deformation. Hence, we conducted experiments to investigate the resistance variation of the conductor at different bending angles. The results of the tests and a schematic diagram of the bending angles (α) are shown in the **Figure 8**. Under the stretching state of 100%, the conductive film was subjected to a bending angle (α) ranging from 0° to 180° . Despite these challenging conditions, the experimental results indicate that the resistance change ratio of the conductive film remained below 0.05%, which confirms the exceptional stability of the conductive film under such complicated deformation scenarios.

In order to illustrate the potential working scenarios of the conductor more vividly, we adhered it onto the wrist and measured its resistance variation rate during wrist bending, as demonstrated in **Figure 9**. Compared with being attached to paper, the wrist is more flexible, and the complex deformation of stretching, bending, and torsion simulates more complicated working conditions. Nevertheless, the conductor still exhibits sufficient resistance stability.

2.3. Practical Application Verification

The performance of stretchable conductors in practical use may be affected by environmental factors such as temperature,

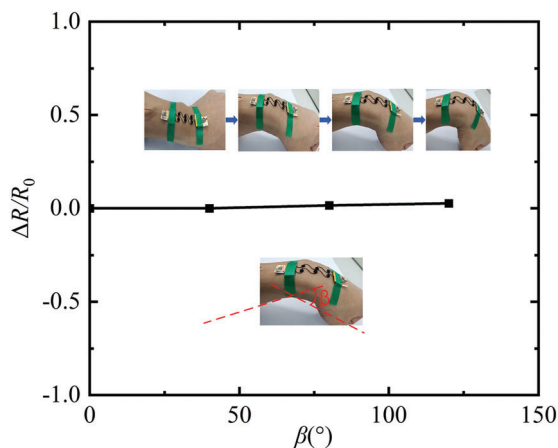


Figure 9. The resistance change ratio of the stretchable conductor under bending wrist.

humidity, working voltage/current, and heat dissipation. It is difficult to fully replicate these conditions in the laboratory, but we selected two typical working scenarios: connecting the conductor to a motor and an LED light, respectively, and observing the changes in the motor's speed and the LED's brightness during stretching.

The experimental photo depicting the connection between the stretchable conductor and the DC motor is presented in **Figure 10**. After connecting the stretchable conductor to the motor and turning on the power, the motor's rotational speed was recorded. Subsequently, the conductor was stretched to strain levels of 50%, 100%, 150%, and 200%, and the variations in motor speed were documented. As shown in **Figure 11**, the speed change ratio were within 0.01%, where n_0 and Δn represent the initial and variation of the motor speed.

The photograph of the LED bulb with increasing strain of the stretchable conductor and the corresponding change in brightness are shown in **Figure 12**. During the process of applying strain from 0% to 200% on the conductor, there was no significant change observed in the brightness of the LED bulb.

2.4. Discussion

The application of the flexible mechanism to the design of stretchable conductors represents an exploratory attempt. Compared to Kirigami-based stretchable conductors, the flexible

mechanism-based stretchable conductor has smaller out-of-plane deformation. Moreover, the resistance change ratio test conducted after the above experiments demonstrates the excellent stability, repeatability, and durability of the flexible mechanism-based stretchable conductor under large strains, verifying the effectiveness of the structure. Additionally, in practical application tests, the stretchable conductor has demonstrated stable current output capabilities, also validating its heat dissipation ability. However, it should be noted that the design of the flexible mechanism-based stretchable conductor is still in its preliminary stage. In future work, we will further optimize the structure and size parameters that can be used for stretchable conductors and investigate the performance changes of the conductor after encapsulation.

3. Conclusions

In summary, this paper proposes a design concept for a highly deformable stretchable conductor inspired by flexible mechanisms. Compared to stretchable conductors based on Kirigami structures, the stretchable conductor based on flexible mechanisms can achieve large in-plane deformation. This paper provides specific examples of the design steps and principles, and verifies the effectiveness of the stretchable conductor based on flexible mechanisms through finite element simulations and experiments. The experimental results demonstrate that the resistance change ratio of the conductor remains within 0.05% during the 0–200% strain process. The consistency and durability of the conductor during stretching deformation were also confirmed through 500 repetitions of the test. Additionally, the experiments with the electric motor and LED light confirm the conductor's ability to maintain a stable current. In conclusion, this paper explores and preliminarily verifies the design of stretchable conductors based on flexible mechanisms.

4. Experimental Section

Materials: TPU granules, high purity hydroxylated multi-walled carbon nanotubes, (TPU : Carbon nanotubes = 8 : 1), and N,N-dimethylformamide (DMF) 20 mL.

Preparation Process of Stretchable Conductor Film: In a glass bottle, 3.3 g TPU granules were weighed and the magnetic agitator rotor was added. Then, 20 mL DMF was added, and the bottle was sealed with plastic wrap and covered. The glass bottle was placed on a magnetic mixer and mixed at a speed of 600 RPM. After one and a half hours, 0.4125 g carbon nanotubes

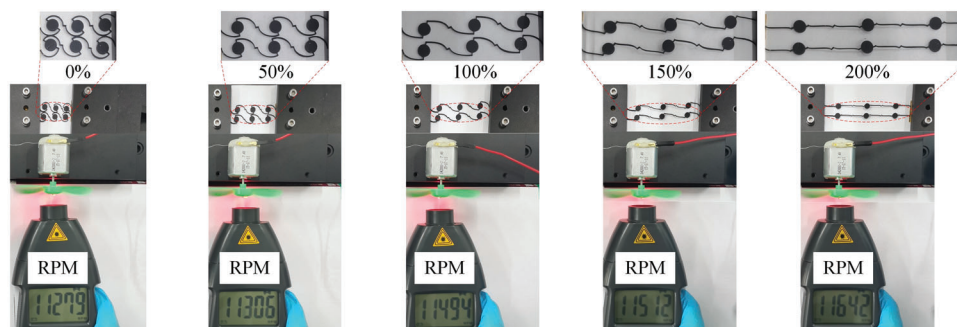


Figure 10. The connection test of the proposed stretchable conductor.

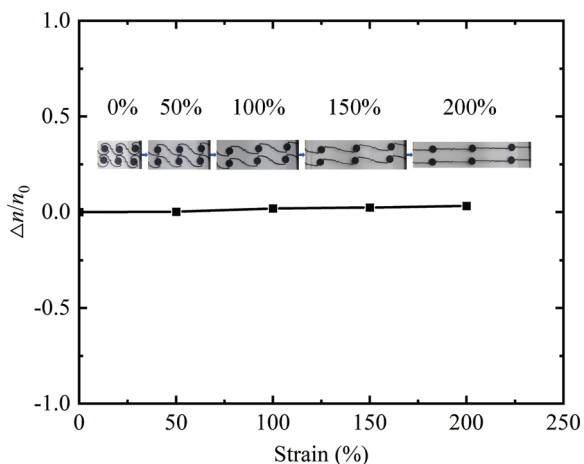


Figure 11. The speed change ratio of the motor under different strain of the conductor.

were added and stirred continuously. This process was repeated twice. The mixture was then placed in an ultrasonic cleaner for 20 min and stirred continuously. Afterward, it was stirred for another 2 h. The solution was poured evenly into two clean petri dishes and left to stand overnight in a 50 °C incubator. The next day, the resting membrane was slowly peeled away from the wall of the dish using tweezers. The resulting film has a rough upper surface and smooth lower surface, is black in color, and is elastic. The overall thickness is about 0.1 mm.

Laser Cutting Process: The designed graphics are imported into the laser cutting software, where the size of the graphics is set (the first two structures are 40.5 mm in length and 20 mm in width; the third structure is 39.5 mm in length and 15 mm in width), and then the object to be cut is selected. The following parameters are set for the laser cutting process: marking speed of 500 mm s⁻¹, air jump speed of 1000 mm s⁻¹, Q frequency of 30 KHz, Q release of 2/mus, 10 marking times, and current of 7A. Due to the minimum distance of the model being 0.4–0.5 mm and the limited accuracy of the laser cutting machine, the model is divided into upper, middle, and lower layers, and partially cut to ensure the cutting quality. Before laser cutting, the frame is previewed and the conductor film is placed in the appropriate position, and both sides are pressed with a steel ruler to prevent position deviation during cutting. Each part is cut accord-

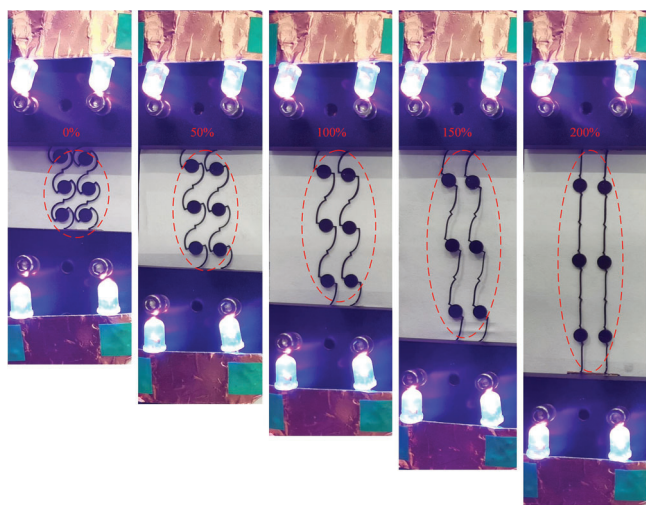


Figure 12. The brightness of LED bulbs under different strains of the conductor.

ing to the actual situation, with 5–7 cutting cycles (50–70 laser markings) until the part is completely cut through before moving on to the next part. After marking, the film is removed and burrs and other adhesive parts are removed with a knife.

Preparation of Stretchable Conductor: The stretchable conductor film was coated on both sides with silver paste and a copper sheet was pasted onto it. The copper sheet was then wrapped around the adhesion of the stretchable conductor on both sides with insulation tape. The sample was then placed in a 60 °C incubator for the silver paste to solidify. Once solidified, the sample was taken out and electrodes were welded onto the copper sheet at both ends.

Conductor Tensile Test: To perform the tensile test, the stretchable conductor was fixed in a circulating drawing instrument, and two electrodes of the conductor were connected with two pens of an oscilloscope. The stretch distance was set based on the tensile ratio (50%–250%) and the actual initial length, and the number of cycle stretches was set to 10 times on the computer. The stretching process was then started, and the oscilloscope recorded the resistance of the stretchable conductor in different states. The data was displayed in the computer software, exported to Excel for subsequent data processing, and finally, the resistance change ratio of the stretchable conductor under different tensile rates was obtained.

Acknowledgements

This work was supported by National Natural Science Foundation of China (Nos. 52205506 and 52205176).

Conflict of Interest

The authors declare no conflict of interest.

Data Availability Statement

The data that support the findings of this study are available from the corresponding author upon reasonable request.

Keywords

conductors, flexible electronics, strain sensors

Received: May 24, 2023

Revised: July 17, 2023

Published online:

- [1] S. Wu, S. Peng, Y. Yu, C.-H. Wang, *Adv. Mater. Technol.* **2020**, *5*, 1900908.
- [2] H. C. Lee, E. Y. Hsieh, K. Yong, S. Nam, *Nano Res.* **2020**, *13*, 1406.
- [3] C. Luo, B. Tian, Q. Liu, Y. Feng, W. Wu, *Adv. Mater. Technol.* **2020**, *5*, 1900925.
- [4] Z. Lou, L. Wang, G. Shen, *Adv. Mater. Technol.* **2018**, *3*, 1800444.
- [5] C. Ma, M. Wang, P. C. Uzabakirho, G. Zhao, *Adv. Mater. Technol.* **2022**, 2200106.
- [6] D.-H. Kim, J.-H. Ahn, W. M. Choi, H.-S. Kim, T.-H. Kim, J. Song, Y. Y. Huang, Z. Liu, C. Lu, J. A. Rogers, *Science* **2008**, *320*, 507.
- [7] Y. Zhang, W. Zhang, G. Ye, Q. Tan, Y. Zhao, J. Qiu, S. Qi, X. Du, T. Chen, N. Liu, *Adv. Mater. Technol.* **2020**, *5*, 1900880.
- [8] H.-Y. Chen, H.-P. Shen, H.-C. Wu, M.-S. Wang, C.-F. Lee, W.-Y. Chiu, W.-C. Chen, *J. Mater. Chem. C* **2015**, *3*, 3318.

- [9] L. Jia, H. Ren, in *Deployable Multimodal Machine Intelligence: Applications in Biomedical Engineering*, Lecture Notes in Bioengineering, (Ed.: H. Ren), Springer Nature, Singapore **2023**, pp. 503–525.
- [10] T. Q. Trung, N.-E. Lee, *J. Mater. Chem. C* **2017**, *5*, 2202.
- [11] M. Wang, P. Baek, A. Akbarinejad, D. Barker, J. Trivas-Sejdic, *J. Mater. Chem. C* **2019**, *7*, 5534.
- [12] Q. Huang, Y. Zhu, *Adv. Mater. Technol.* **2019**, *4*, 1800546.
- [13] Y. Wang, Z. Wang, Z. Wang, T. Xiong, P. P. Shum, L. Wei, *Adv. Electron. Mater.* **2023**, *9*, 2201194.
- [14] J. Park, J. S. Myung, D. Cho, T. Kim, S. Y. Lee, Y. Kim, Y. Choi, S. Jung, *Adv. Electron. Mater.* **2023**, *9*, 2370007.
- [15] X. Wu, Y. Han, X. Zhang, C. Lu, *ACS Appl. Mater. Interfaces* **2017**, *9*, 23007.
- [16] T. Wang, R. Wang, Y. Cheng, J. Sun, *ACS Appl. Mater. Interfaces* **2016**, *8*, 9297.
- [17] P. Wang, B. Sun, Y. Liang, H. Han, X. Fan, W. Wang, Z. Yang, *J. Mater. Chem. A* **2018**, *6*, 10404.
- [18] Q. Ma, Y. Zhang, *J. Appl. Mech.* **2016**, *83*, 11.
- [19] S. Shafiqat, J. P. M. Hoefnagels, A. Savov, S. Joshi, R. Dekker, M. G. D. Geers, *Micromachines* **2017**, *8*, 277.
- [20] J. Lyu, M. D. Hammig, L. Liu, L. Xu, H. Chi, C. Uher, T. Li, N. A. Kotov, *Appl. Phys. Lett.* **2017**, *111*, 161901.
- [21] Z. Wang, L. Zhang, S. Duan, H. Jiang, J. Shen, C. Li, *J. Mater. Chem. C* **2017**, *5*, 8714.
- [22] K. Yong, S. De, E. Y. Hsieh, J. Leem, N. R. Aluru, S. Nam, *Mater. Today* **2020**, *34*, 58.
- [23] P. Won, J. J. Park, T. Lee, I. Ha, S. Han, M. Choi, J. Lee, S. Hong, K.-J. Cho, S. H. Ko, *Nano Lett.* **2019**, *19*, 6087.
- [24] K. Xu, Y. Lu, S. Honda, T. Arie, S. Akita, K. Takei, *J. Mater. Chem. C* **2019**, *7*, 9609.
- [25] T. C. Shyu, P. F. Damasceno, P. M. Dodd, A. Lamoureux, L. Xu, M. Shlian, M. Shtein, S. C. Glotzer, N. A. Kotov, *Nat. Mater.* **2015**, *14*, 785.
- [26] R. Sun, B. Zhang, L. Yang, W. Zhang, I. Farrow, F. Scarpa, J. Rossiter, *Appl. Phys. Lett.* **2018**, *112*, 251904.
- [27] A. Lamoureux, K. Lee, M. Shlian, S. R. Forrest, M. Shtein, *Nat. Commun.* **2015**, *6*, 8092.
- [28] R. Xu, A. Zverev, A. Hung, C. Shen, L. Irie, G. Ding, M. Whitmeyer, L. Ren, B. Griffin, J. Melcher, L. Zheng, X. Zang, M. Sanghadasa, L. Lin, *Microsyst. Nanoeng.* **2018**, *4*, 3.
- [29] M. Gonzalez, F. Axisa, M. Vanden Bulcke, D. Brosteaux, B. Vandeveldel, J. Vanfleteren, in *2007 Int. Conf. on Thermal, Mechanical and Multi-Physics Simulation Experiments in Microelectronics and Micro-Systems. EuroSime 2007*, IEEE, Piscataway, NJ **2007**, pp. 1–6.
- [30] L. L. Howell, *Compliant Mechanisms*, John Wiley & Sons, Inc, New York **2001**.
- [31] K. Lu, Y. Tian, C. Liu, C. Zhou, Z. Guo, F. Wang, D. Zhang, B. Shirinzadeh, *Int. J. Mech. Sci.* **2020**, *186*, 105895.
- [32] Y. Tian, K. Lu, F. Wang, C. Zhou, Y. Ma, X. Jing, C. Yang, D. Zhang, *IEEE/ASME Trans. Mechatron.* **2020**, *25*, 1322.
- [33] S. He, H. Tang, K. Zhang, C. Chen, J. Wang, Z. Zhu, J. Gao, C. Cui, X. Chen, *IEEE Trans. Ind. Electron.* **2021**, *68*, 2345.
- [34] H. Li, B. Zhu, X. Zhang, J. Wei, S. Fatikow, *IEEE Trans. Ind. Electron.* **2021**, *68*, 3324.
- [35] N. Lobontiu, E. Garcia, *Comput. Struct.* **2003**, *81*, 1329.
- [36] J. M. Paros, L. Weisbord, *Mach. Des.* **1965**, *37*, 151.
- [37] N. Lobontiu, J. S. N. Paine, E. Garcia, M. Goldfarb, *J. Mech. Des.* **2000**, *123*, 346.
- [38] B. Ji, X. Wang, Z. Liang, H. Zhang, Q. Xia, L. Xie, H. Yan, F. Sun, H. Feng, K. Tao, Q. Shen, E. Yin, *Int. J. Human–Comput. Interaction* **2023**, *0*, 1.
- [39] Y. Lee, A. Carnicer-Lombarte, S. Han, B. J. Woodington, S. Chai, A. G. Polyvas, S. Velasco-Bosom, E.-H. Kim, G. G. Malliaras, S. Jung, *Adv. Mater.* **2023**, *n/a*, 2301782.
- [40] H.-H. Pham, I.-M. Chen, *Precis. Eng.* **2005**, *29*, 467.